MDPI

Article

Model-Scale Reproduction of Fan Pressurization Measurements in a Wind Tunnel: Design and Characterization of a New Experimental Facility

Adeline Mélois [1,*][ID], Anh Dung Tran [1,2][ID], Bassam Moujalled [1][ID], Mohamed El Mankibi [2][ID], Gaëlle Guyot [1][ID], Benedikt Kölsch [1,3][ID] and Valérie Leprince [3]

1   BPE Research Team—Cerema, 46 rue Saint Théobald, 38080 L'Isle d'Abeau, France; anhdung.tran@univ-evry.fr (A.D.T.); bassam.moujalled@cerema.fr (B.M.); gaelle.guyot@cerema.fr (G.G.); benedikt.koelsch@cerema.fr (B.K.)
2   ENTPE LTDS, 3 rue Maurice Audin, 69518 Vaulx-en-Velin, France; mohamed.elmankibi@entpe.fr
3   Direction Territoire et Ville—Cerema, 2 rue Antoine Charial, 69426 Lyon, France; valerie.leprince@cerema.fr
*   Correspondence: adeline.melois@cerema.fr

Abstract: In many countries, building airtightness is mandated by national regulations or energy efficiency programs, necessitating accurate measurements using the fan pressurization method. Given the significant influence of wind on measurement uncertainty and the need for reliable regulatory tests, experimental studies in a controlled environment are needed. This paper presents a novel experimental facility designed to replicate fan pressurization measurements on a model scale under controlled laboratory conditions. The key features of the facility include the ability to (1) conduct fan pressurization measurements, (2) generate steady wind conditions across varying wind speeds, and (3) accurately measure parameters like the pressure difference, wind speed, and airflow rate. The experimental facility includes a pressurization device, a wind tunnel, and a model representing a two-story house with nine distinct leakage distributions. A total of 96 fan pressurization measurements were executed using this setup, adhering to the similarity conditions specifically defined for assessing airflow errors due to wind. These tests followed the ISO 9972 standard, with the pressure differences ranging from 10 Pa to 100 Pa and steady wind speeds from $1 \text{ m} \cdot \text{s}^{-1}$ to $7.5 \text{ m} \cdot \text{s}^{-1}$. This experimental facility marks a significant advancement in understanding the effect of wind on building airtightness measurements.

Keywords: building airtightness; measurement; wind tunnel; model; wind impact

1. Introduction

1.1. Building Airtightness: A Key Factor for Building Energy Performance and Indoor Air Quality

In line with the European Directive 2010/31/EU, new buildings in Europe aim to reach near-zero energy levels [1]. Moreover, the European Commission has proposed for all new buildings to be carbon neutral by 2030. Given the challenges posed by global warming, researchers, builders, manufacturers, and other stakeholders are gathering their forces to maintain good indoor quality and acceptable thermal comfort in buildings with minimal energy and environmental impact. Recognizing the significance of these challenges, minimizing and controlling building envelope air leakage has become one of the major levers for reducing energy consumption in buildings. Since the 1970s, many studies have highlighted the impact of poor airtightness on building energy consumption. More recently, Amanowicz et al. [2] presented new studies that confirm the energy impact of buildings' airtightness. In particular, Simson et al. evaluated the infiltration heat losses for two reference cases in Estonia [3] and estimated that they represent, in most cases, 13 to 16% of the total building heat losses but can reach 50% for the highest wind speeds configuration. In Spain, Poza-Casado et al. conducted a study using more than 400 blower

door tests performed on Spanish dwellings over several periods and locations [4]. They estimated that infiltrations can induce energy consumption due to heating demand from 2.43 to 19.07 kW h/(m^2 y). Given the critical role of airtightness for achieving the energy performance targets of buildings, particularly as low-energy goals become more ambitious, many countries include requirements for building airtightness in their national regulations or energy efficiency programs [5]. Among them, some require justification of the respect of a threshold value for a building airtightness indicator, such as q_{a4} ($Q_{4Pa\text{-}surf}$ in French: the air leakage rate at 4 Pa divided by the loss surface area excluding the basement floor) in France and ELA_4 (equivalent leakage area at 4 Pa) in the U.S. as low-pressure difference indicators or n_{50} (air change rate at 50 Pa) and q_{50} (air leakage rate at 50 Pa) as high-pressure difference indicators, used in many countries like Germany, Ireland, Poland, and the U.K. [5,6]. This justification commonly consists of a fan pressurization measurement performed at commissioning. Moreover, the infiltration may have a significant impact on the efficiency of ventilation systems, and thus on the indoor air quality. As presented by Kempton et al. in their review paper [7], increasing the airtightness of buildings may have a positive impact on the indoor air quality by reducing the infiltration of particles and leading to lower NO_2 concentrations indoors, in addition to improving the efficiency of the ventilation system.

1.2. Background of the Fan Pressurization Measurement Method

Air leakage measurements are mainly performed using the fan pressurization method, as described in the standards like ISO 9972 [8] and ASTM 779-19 [9]. These tests are conducted extensively worldwide, with a considerable number documented in databases. LBNL's residential diagnostics database (ResDB) included 75,000 entries in 2013 [10], French's national database of measurements performed in France by qualified testers included about 570,000 measurements in 2023 [6], and the U.K.'s ATTMA database included 192,731 records in 2017 [11].

Typically, the relation between the airflow through building envelopes or building components and the indoor–outdoor pressure is given by the power law [12].

$$q = C * \Delta p^n \tag{1}$$

where q is the volumetric airflow rate (m^3·s^{-1}), C is the leakage coefficient (m^3·h^{-1} Pa^{-n}), Δp is the inside–outside pressure difference (Pa), and n is the airflow exponent (-).

The purpose of the fan pressurization measurement method lies in measuring the airflow rate for a reference indoor–outdoor pressure difference. This involves either extracting air from the building or supplying air to it to maintain a range of pressure differences.

ISO 9972 requires the following:

1. A zero-flow pressure difference (between inside and outside) should be recorded both before and after the pressure sequence. Each measurement must last for at least 30 s and include at least 10 points. The result, represented as $\Delta p0$, is the average of all the zero-flow pressure differences values.
2. For the pressure sequence, the following conditions are required:
3. The lowest pressure difference must be at least 10 Pa or $5\Delta p0$, whichever is greater.
4. The highest pressure difference must be at least 50 Pa, but 100 Pa is recommended.
5. The difference between each successive reading must not exceed approximately 10 Pa.
6. The sequence must include at least five approximately equally spaced tests.
7. Through the analysis of these pressure differences and the associated airflow rates, the values of C and n can be ascertained using a linear regression applied to $\ln(q)$ and $\ln(\Delta p)$. From this, the airflow rate for the reference pressure difference can be extrapolated.

1.3. Need to Better Characterize the Measurement Reliability

Building pressurization measurements are increasingly used for compliance checks for energy performance requirements, and non-compliance may result in severe penalties [13].

Given this, understanding the uncertainty of the measurement results has become a key concern in several countries over the past few years, especially for indicators at 4 Pa, which are more sensitive to changes in environmental conditions [14].

Numerous studies have shown significant uncertainties induced by the wind, as shown by the review document recently published by Leprince and Hurel [15]. Some of these studies were based on analytical models that significantly simplified the physics, such as the single-zone model with two leaks used by Carrié and Leprince [16] and the Monte Carlo simulations conducted by Delmotte to understand and assess the systematic measurement error induced by steady wind and the stack effect generated by systematic measurement error [17]. To the author's knowledge, no existing tool can simulate a building undergoing a pressurization measurement according to ISO 9972. While some tools like CONTAM attempt such modeling, their methods remain simplistic, often including only a single airflow measurement at a unique pressure difference. Another crucial assumption concerns the pressure coefficients, which are typically derived from wind tunnel tests for simplified geometries of buildings, potentially misrepresenting real-world scenarios.

Other studies involved field measurements performed on a small number of buildings that characterized the impact of the wind only for the specific situations of these buildings, such as the study conducted by Walker et al. From 6007 measurements performed on six test houses in various wind speed conditions in Canada [10], the previous study was performed on one of these tests houses by Modera and Wilson [18]. In 2011, Delmotte and Laverge evaluated the repeatability and reproducibility of the test method from the measurements performed on one building in Belgium [19]. Later, Prignon et al. analyzed 31 tests on a newly constructed apartment within a period of 15 days in October 2017 for a study dedicated to pressure measurements [20]. They used the same experimental data to quantify the impact of changing the regression technique [21]. Kölsch and Walker also worked on the impact of the data analysis method used in the standard [22]. There remains a need for further investigations to better understand the physics during airtightness measurements, as explained by Kölsch et al. [23]. More specifically, it is necessary to understand how the wind affects pressurization measurements to characterize the error induced by the wind on the measurement results. This investigation would necessitate reproducing various wind conditions with detailed knowledge of the buildings' airtightness for varying leakage distributions. Moreover, an accurate measurement device is essential.

One less expensive and more technically feasible alternative to real-scale measurements is the use of model-scale experiments. Such an approach allows for controlled wind conditions on a model for which the exact envelope airtightness is known. This helps assess the error induced by the wind on a measurement result. Furthermore, these model-scale experiments offer the possibility of studying various configurations of wind speeds and air leakage distributions in laboratory conditions. To accurately study the wind impact on fan pressurization measurements using a model, it is necessary to define the physical properties being studied in order to define the similarity conditions. This ensures that the results from the model scale can be faithfully translated into real-scale applications.

1.4. Objective

The goal of this study was to unveil an experimental facility tailored to evaluating the impact of steady wind on building airtightness measurements and explore strategies to reduce the measurement uncertainty attributed to wind effects. This entailed the following objectives:

- Executing fan pressurization measurements on a model scale.
- Simulating steady wind scenarios at different wind speeds.
- Accurately measuring the parameters, such as the pressure differences, wind speeds, and airflow rates.

In alignment with these objectives, the experiment facility will include the following.

- A model of a single-zone building on a model scale.
- A pressurization measurement device mirroring a blower door on a model scale.

- A wind tunnel to simulate steady wind conditions.
- The necessary sensors and actuators.

The subsequent sections of this paper delineate the experimental facility's design and installation, as well as the findings from the tests for various leakage distributions, the evaluation of the wind in the testing chamber of the wind tunnel, and the presentation of the fan pressurization measurements. The limits and the future evolutions of the experimental facility are detailed in the discussion section.

2. Materials and Methods: Design of the Model-Scale Experiment

The reproduction of physics on a reduced model necessitates an adherence to similarity conditions between the full scale and the reduced scale. Only when these similarity conditions are satisfied can the results obtained on a reduced scale be applied to a full scale. These conditions are defined in this section, built upon equations presented in detail in a previous work by Carrié and Mélois [24]. Section 2.1 derives non-dimensional numbers from these equations, ensuring the conservation of the values of these numbers across the scales to guarantee similarity. Section 2.2 is dedicated to the definition of the scale ratios, which led to the design of the experimental facility. Section 2.3 defines the sizes of each component of the wind tunnel, Section 2.4 presents the characteristics of the model, and Section 2.5 describes the pressurization device that fits the model scale. This work has been partially described by Mélois et al. [25,26].

2.1. Definition of Similarity Conditions

To respect the similarity conditions between real-scale measurements and model-scale experiments, a dimensional analysis identifies dimensionless numbers. The conservation of the values of these numbers across the scales will ensure similarity. Employing a method described by N. Le Roux [27], a reference value X_{ref} was introduced for each dimensional variable X within Equations (2)–(6). Table 1 defines the X_{ref} reference value for each variable in these equations.

Table 1. Definition of the reference values and dimensionless variables.

	Variable	X_{ref} Reference Values	Dimensionless Variable
p	Pressure	p_{ref}	$p^* = \frac{p}{p_{ref}}$
ρ	Air density	ρ_{ref}	$\rho^* = \frac{\rho}{\rho_{ref}}$
U	Wind speed at the height of the building	U_{ref}	$U^* = \frac{U}{U_{ref}}$
A	Area of opening	A_{ref}	$A^* = \frac{A}{A_{ref}}$
V_i	Internal building volume	$V_{i\,ref}$	$V_i^* = \frac{V_i}{V_{i\,ref}}$
q	Volumetric airflow rate	q_{ref}	$q^* = \frac{q}{q_{ref}}$
t	Time	t_{ref}	$t^* = \frac{t}{t_{ref}}$

In accordance with Carrié and Leprince [16], the building was represented by a single zone separated from the outside by two types of walls: walls on the windward side of the building, which were subject to the same upwind pressure, and walls on the leeward side, which were subject to the same downwind pressure. Furthermore, it was assumed that all the leaks on the windward (respectively, leeward) side could be represented as a single opening at a given height on the windward side (respectively, leeward) subjected to the same pressure difference. Thus, a specific configuration with two identical openings (same

size and same height) under isothermal initial conditions and with a steady wind provided one general equation (Equation (2)) for both openings.

$$\Delta p = C_p \frac{\rho U^2}{2} - p_{in} \tag{2}$$

where Δp is the pressure difference between inside and outside at the opening (Pa), C_p is the wind pressure coefficient at the opening (-), ρ is the air density (kg m^{-3}), U is the wind speed at the height of the building (m·s^{-1}), and p_{in} is the indoor pressure relative to the external pressure (Pa).

By replacing each variable with the respective dimensionless and reference variables, the first dimensionless numbers were obtained, as shown in bold in Equation (3).

$$\Delta p^* = \left(\frac{\rho_{ref}.U_{ref}^2}{p_{ref}} \right).C_p \frac{\rho^*.U^{*2}}{2} - p_{in}^* \tag{3}$$

Similarly, one general flow equation (Equation (4)) was considered for the two openings, in which dimensionless variables could be introduced.

$$\frac{4C_d A^{\frac{3}{2}}}{\sqrt{\pi}} \frac{dq(t)}{dt} = -q^2(t)sign(q(t)) + 2C_d^2 A^2 \frac{\Delta p(t)}{\rho} \tag{4}$$

where C_d is the discharge coefficient of the opening, A is the area of the opening (m^2), q is the volumetric airflow rate through the opening (m^3·s^{-1}), Δp is the pressure difference between inside and outside at the opening, and ρ is the air density (kg m^{-3}).

The reference time was defined as follows: $t_{ref} = \frac{L_{ref}}{U_{ref}}$, where L_{ref} is a characteristic length. The second and third dimensionless numbers are shown in bold in Equation (5).

$$\frac{\sqrt{A_{ref}}}{L_{ref}}.\sqrt{\frac{p_{ref}.A_{ref}^2}{\rho_{ref}.q_{ref}^2}}.\sqrt{\frac{\rho_{ref}.U_{ref}^2}{p_{ref}}}.\frac{4.C_d.A^{*\frac{3}{2}}}{\sqrt{\pi}}.\frac{dq^*}{dt^*} = -q^{*2}sign(q^*) + \frac{p_{ref}.A_{ref}^2}{\rho_{ref}.q_{ref}^2}2C_d^2.A^{*2}\frac{\Delta p^*}{\rho^*} \tag{5}$$

The fourth dimensionless numbers were obtained in bold in Equation (6) using the mass balance equation.

$$\left(\frac{V_{ref}.U_{ref}}{L_{ref}.q_{ref}} \right) V_i^* \frac{d\rho^*}{dt^*} = \sum \rho^*.q^* \tag{6}$$

As a result, four dimensionless numbers presented in Equations (7)–(10) were identified.

$$\Pi_1 = \frac{\rho_{ref}.U_{ref}^2}{p_{ref}} \tag{7}$$

$$\Pi_2 = \frac{p_{ref}.A_{ref}^2}{\rho_{ref}.q_{ref}^2} \tag{8}$$

$$\Pi_3 = \frac{\sqrt{A_{ref}}}{L_{ref}} \tag{9}$$

$$\Pi_4 = \frac{V_{ref}.U_{ref}}{L_{ref}.q_{ref}} \tag{10}$$

2.2. Definition of Scale Ratios

To reach similarity conditions, the values of the dimensionless numbers Π_1 to Π_4 must be identical both on the model and real scale. For each variable, the scale ratio $\overline{X}$ was defined according to Equation (11).

$$\overline{X} = \frac{X_{ref\ model}}{X_{ref\ real}} \tag{11}$$

Assuming that the air had the same properties on both scales, the scale ratio of the air densities was equal to 1. Therefore, the conservation of Π_1 to Π_4 led to the four relations between the scale ratios, as shown in Equations (12)–(15).

$$\overline{U}^2 = \overline{p} \tag{12}$$

$$\overline{p}.\overline{A}^2 = \overline{q}^2 \tag{13}$$

$$\overline{A}^{0.5} = \overline{L} \tag{14}$$

$$\overline{V}.\overline{U} = \overline{L}.\overline{q} \tag{15}$$

To design a model fitting into a wind tunnel, the scale ratio for the length must be fixed. This directly defined the scale ratios for the areas using Equation (14). According to the systems defined by Equations (12)–(15), another scale ratio could be fixed. Setting a scale ratio for the wind speed $\overline{U} = 1$ fixed the scale ratio for pressure $\overline{p} = 1$. This implied that the experimental facility would replicate real-scale wind speeds and pressure differences.

The study presented in this paper considered only steady wind, where the equations were simpler and all the variables did not depend on time. Thus, Equation (5) became (16) and Equation (6) became (17).

$$-q^{*2}sign(q^*) + \frac{p_{ref}.A_{ref}^2}{\rho_{ref}.q_{ref}^2} 2C_z^2.A^{*2}\frac{\Delta p^*}{\rho^*} = 0 \tag{16}$$

$$\sum \rho^*.q^* = 0 \tag{17}$$

To respect the laboratory constraints regarding the sizes, a scale ratio of $\overline{L} = 1/25$ was selected for the length. In the context of steady winds, only dimensionless numbers Π_1 and Π_2 had to be conserved to satisfy the similarity conditions. However, as the experimental facility was meant to be used for future studies, the relations between the scale ratios as defined in the general situation were considered. Thus, the scale ratio for the area was $\overline{A} = (1/25)^2$, the scale ratio for the volume was $\overline{V} = (1/25)^3$, and the scale ratio for the volumetric airflow was $\overline{q} = (1/25)^2$.

2.3. Wind Tunnel Components

The ISO 9972 standard indicates that, for meteorological wind speeds above $6\ m\cdot s^{-1}$, the zero-flow pressure difference requirement (one of the requirements defined in this standard for performing such a valid measurement) is unlikely to be respected. To evaluate the relevance of this requirement, the wind speed was adjusted between 0 and at least $7\ m\cdot s^{-1}$. Therefore, the wind tunnel was engineered to provide a steady wind from 0 to at least $7\ m\cdot s^{-1}$ within the testing chamber. Given this range for the wind speed, the wind tunnel was classified as a "low-speed wind tunnel" [28]. The wind tunnel was then designed according to the methodology explained by Mauro et al. [29], including five key components:

1. Settling chamber. This included a honeycomb and two screens. The porosity of the honeycomb was 0.8, and the ratio between length and hydraulic diameter was 7.5, as recommended by [29]. The first screen was made of galvanized steel with a porosity of 0.64, whereas the second was made of steel with a porosity of 0.74, according to Prandtl [30].

2. Contraction component. This unit had dual purposes: (1) accelerating the flow in the testing chamber and (2) providing a uniform flow velocity profile inside the testing chamber. A preliminary design carried out according to [31,32] yielded a simplified shape using 30° inclined planes, selected for its balance between a small deviation in the velocity field in the flow direction (less than 3% deviation from the Bell-Mehta form) and fabrication ease.

3. Testing chamber (TC). This tunnel segment stabilized and achieved the target wind speed. The area of the cross-section measured 1.0×1.0 m^2 in order to fit into the laboratory. To install the model and different sensors easily, the length of the TC was set to 1.5 m, in line with the conditions given by Mauro et al. [29].

4. Fan. To generate wind speeds up to 7 m·s^{-1} in the cross-section of the testing chamber of 1 m^2, the fan will need to provide an airflow rate up to 7.0 m^3·s^{-1}. The wind tunnel included an axial fan with a maximum airflow rate of around 11.9 m^3·s^{-1}, depending on the pressure drop. This fan, with a diameter of 1.0 m, could be controlled with a frequency converter.

5. Diffuser. As the fan's diameter was the same size as the testing chamber, a length of 0.5 m was sufficient for the diffuser between the testing chamber and the fan.

Figure 1 shows the key components of the wind tunnel, which was 4.11 m long with a maximal cross-sectional area of 4.0 m^2 for the settling chamber and 1 m^2 for the testing chamber.
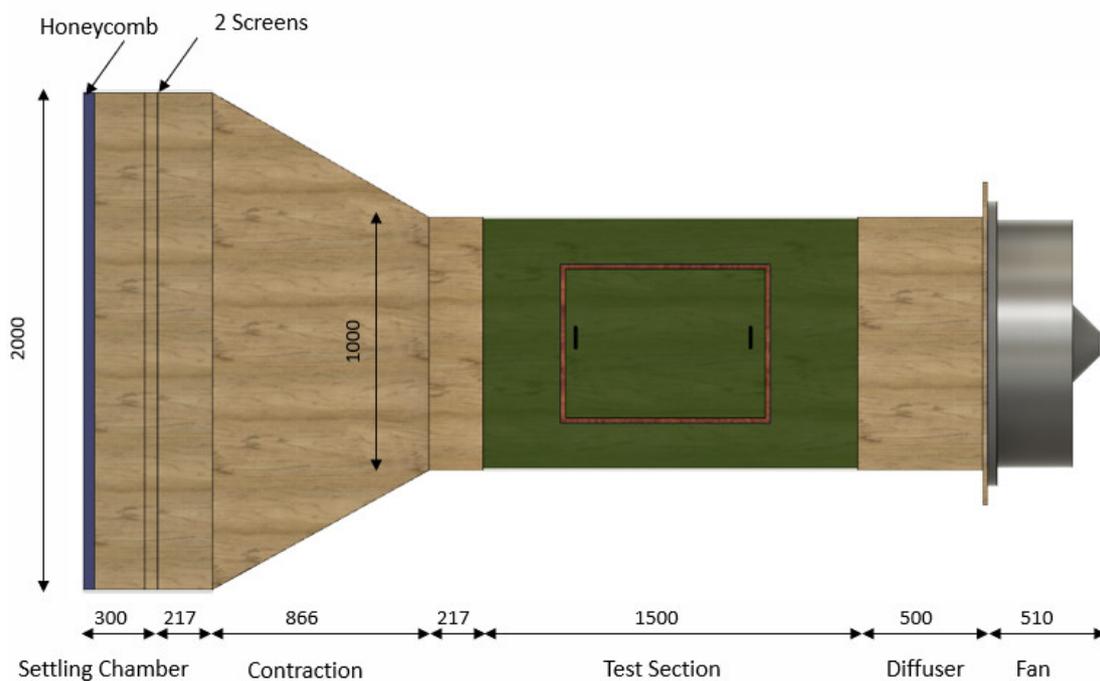

Figure 1. Side view of the final design of the wind tunnel. The dimensions are given in mm.

Figure 2 shows the wind tunnel. The wind tunnel was installed in a 4.60×6.75 m^2 dedicated room. The wall behind the settling chamber of the wind tunnel was more than 1 m away from the honeycomb, which respected a half-diameter limit. Therefore, it did not disturb the flow inside the wind tunnel. The wind velocity was recorded by a directional hot wire anemometer installed at 0.25 m from the ground and at the entry of the testing chamber (windward side). The pressure reference was recorded by a manometer connected to a pressure tap installed next to the anemometer.
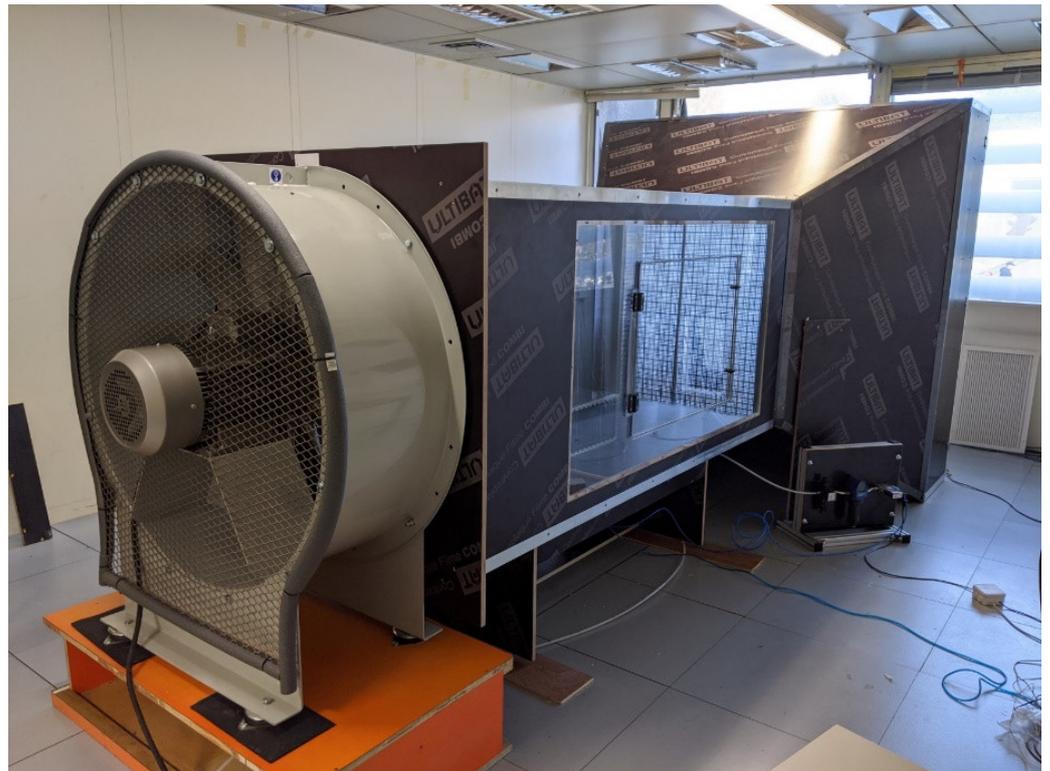
Figure 2. Installed wind tunnel.

2.4. Single-Zone Scale Model

The study focused on a generic two-story house, as illustrated in Figure 3 (left). Its effective leakage area (ELA$_4$) was 0.0142 m^2, aligning with the limit value required for new houses in the current French EP regulation (RE2020). To avoid the need for blockage analysis and correction in the testing chamber of the wind tunnel, the cross-section of the building model had to be below 5% of the testing chamber cross-section (0.05 m^2). This limit was defined by the ASCE, as indicated by Choi and Kwon (1998) [33]. The cross-section of the real house was 6.0 × 5.0 = 30.0 m^2. Using a scale ratio of 1/25, the cross-section of the model was 0.20 × 0.24 = 0.048 m^2, respecting the 5% limit. The model dimensions are presented in Figure 3 (right).
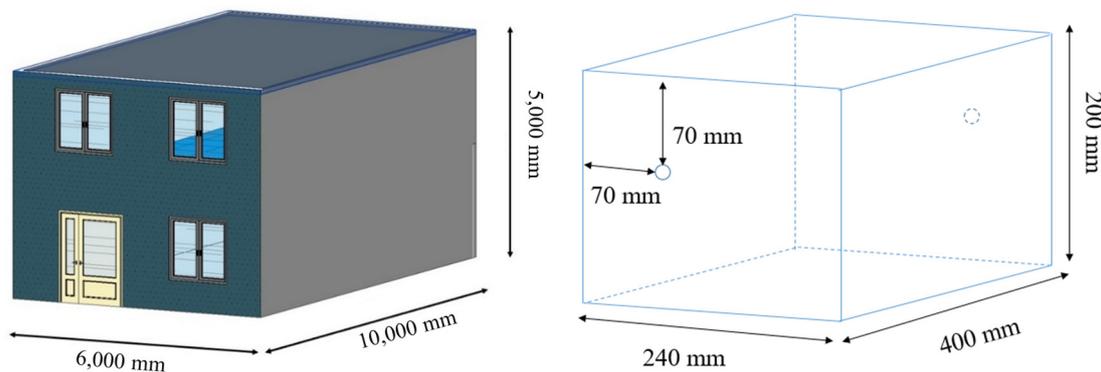

Figure 3. Generic two-story house at a real scale (**left**) and a reduced model at a 1/25 scale (**right**).

However, it is important to note that this simplified model did not encompass the complexities introduced by varying the roof geometries, protruding elements such as chimneys or sewage pipes, and environmental factors like nearby buildings or vegetation. These aspects can significantly influence the pressure distribution and, consequently, the airtightness measurements. Studies [34,35] indicated that the shape and geometry of a building,

along with its surrounding environment, are critical factors affecting surface pressures and wind flow patterns. Therefore, while our cuboid model provided foundational insights, the results may not directly translate to buildings with more complex geometries or in different environmental settings. In future research, we aim to include models with varied roof shapes and protruding elements and account for the influence of surrounding structures and natural features. This approach would necessitate recalculating the similarity numbers and potentially refining the modeling process to accurately represent these additional complexities. Such research would extend the applicability of our findings and contribute to a more comprehensive understanding of the impact of wind on building airtightness across a wider range of architectural designs and environmental contexts.

In terms of the leakage dimensions, using a scale ratio of 1/25 provided an effective leakage area of 22.7 mm^2 at the scale of the model. As explained in Section 2.1, this leakage area was distributed into two openings, one on the windward façade and the other one on the opposite leeward façade. Each opening was perfectly circular. Although this did not completely represent common leaks in building envelopes, each opening was perfectly circular. Although this does not completely represent common leaks of building envelopes, this design offered the advantage of effectively characterizing the airflow. Carrie and Leprince [16] showed that while the total leakage area is not an influential parameter in the evaluation of the impact of the wind, the distribution of the leaks between the windward and leeward façades significantly impacts wind-induced errors. Therefore, the model included different leak sizes to study different leakage distributions. A leakage distribution ratio r_{LD} was defined according to Equation (18).

$$r_{LD} = \frac{A_1}{A_1 + A_2} \tag{18}$$

where r_{LD} is the leakage distribution ratio and A_1 and A2 are the areas of openings one and two, respectively (m^2).

As the leakage distribution in real buildings is extremely variable [36], nine configurations were considered from $r_{LD} = 0.1$ to $r_{LD} = 0.9$. Table 2 presents the diameters of the windward and leeward leaks for these configurations.

Table 2. Diameters of the building model openings for different leakage distribution ratios.

Windward leak size [% of ELA$_4$]	10	20	30	40	50	60	70	80	90
Windward leak diameter [mm]	1.7	2.4	2.9	3.4	3.8	4.2	4.5	4.8	5.1
Leeward leak size [% of ELA$_4$]	90	80	70	60	50	40	30	20	10
Leeward leak size diameter [mm]	5.1	4.8	4.5	4.2	3.8	3.4	2.9	2.4	1.7

To minimize boundary layer turbulence and the impact of the openings on each other, both openings were located 130 mm away from the bottom of the model and 70 mm away from the right-hand side of each façade, as seen in Figure 3 (right).

The model's construction utilized a metal frame, complemented by removable Plexiglax$^®$ façades fixed to the frame with screws and seals (Figure 4 (left)). The two façades with the openings included a large circular opening (Figure 4 (middle)). Several metallic disks were designed (Figure 4 (right)), each tailored to the diameters defined in Table 2. These disks were plugged into the large circular openings like corks. To allow for accurate measurements of the physical parameters inside the model, the floor of the model included the following:

- Taps for the pressure differences measurements or model pressurization.
- Seven circular airtight openings for inserting devices like thermometers. Each of these openings featured a sealing mechanism to ensure absolute airtightness when the opening was not used.

Figure 4. Side view in the model (**left**), front view of the model (**middle**), and the metallic openings (**right**).

2.5. Pressurization Device

In order to investigate the wind impact under various conditions, the pressurization device must be able to achieve the following:

1. Impose pressure differences from 10 to 100 Pa across all leak configurations and wind speeds up to 7 m·s^{-1}.
2. Accurately measure the supplied airflow rate.
3. Fit into the building model.

As the leaks were circular openings, the discharge coefficients were assumed to be $C_{d,1} = C_{d,2} = 1.0$. Regarding the pressure difference evaluation, the following pressure coefficients were considered: $C_{p,1} = 0.5$ and $C_{p,2} = -0.7$ [37]. For each leak distribution configuration, wind speed, and pressure difference imposed by the pressurization device, the theoretical airflow provided by the pressurization device was calculated according to the equations defined by Carrié and Mélois [24] in steady conditions.

Table 3 gives the maximum and minimum airflow rates the pressurization device should provide depending on the leak distribution, considering wind speeds from 0 to 7 m·s^{-1} and pressure difference from 10 to 100 Pa. The range of this airflow was also set to $[3.0 \times 10^{-5}$ m^3·s^{-1}; 3.0×10^{-4} m^3·s$^{-1}]$.

Table 3. Evaluation of airflow provided by the pressurization device depending on the leak distribution ratio.

Leak Distribution Configuration *	90/10	80/20	70/30	60/40	50/50	40/60	30/70	20/80	10/90
$q_{bd,\ max}$ [m^3·s^{-1}]	2.5×10^{-4}	2.5×10^{-4}	2.5×10^{-4}	2.5×10^{-4}	2.5×10^{-4}	2.5×10^{-4}	2.6×10^{-4}	2.6×10^{-4}	**2.7×10^{-4}**
$q_{bd,\ min}$ [m^3·s^{-1}]	**3.8×10^{-5}**	5.0×10^{-5}	6.1×10^{-5}	7.2×10^{-5}	8.4×10^{-5}	9.3×10^{-5}	9.3×10^{-5}	9.3×10^{-5}	9.3×10^{-5}

* windward leak area/leeward leak area [% total area].

The pressurization device included a flow controller (Bronkhorst—EL-FLOW Select—F-201AV-50K-ABD-33-V), as shown in Figure 5 (left). This equipment aligned with the design requirements, providing airflow rates from 6.7×10^{-6} m^3·s^{-1} to 1.7×10^{-3} m^3·s^{-1}. Its uncertainty was the maximum between $\pm 5\%$ of the measured value and $\pm 1.6 \times 10^{-6}$ m^3·s^{-1}. The flow controller was connected to a compressor (Figure 5 (middle)) that provided air at a pressure of 3.0×10^5 Pa. The flow controller was controlled using the LabVIEW environment. The tailored application set the target airflow supplied in the model depending on the pressure difference measured by a manometer (Figure 5 (right)).

Figure 5. Pressurization device for the model-scale measurement with an airflow controller (**left**), a compressor (**middle**), and a manometer (**right**).

2.6. Synthesis of Measured Parameters

For each variable measured in the experimental facility, Table 4 presents the measurement equipment used and its accuracy.

Table 4. Measuring device information.

Measured Variable	Measuring Device	Measuring Range	Accuracy
Wind velocity in the wind tunnel U [m·s^{-1}]	Hot Wire Anemometer HD430TS	0–40 m·s^{-1}	±0.2 m·s^{-1}
Pressure difference ΔP *(between inside the wind tunnel and inside the model)*	Digital pressure gauge APT4	0–1000 Pa	≤1% (0–800 Pa) ≤2% (800–1000 Pa)
Temperature T *(inside the wind tunnel and inside the model)*	PT100 Temperature sensor	−40 °C–+105 °C	≤±0.8 °C
Airflow rate q insufflated inside the model	Mass airflow controller Bronkhorst—EL-FLOW Select—F-201AV-50K-ABD-33-V	[6.7 × 10^{-6} m^3·s^{-1}; 1.7 × 10^{-3} m^3·s^{-1}]	MAX [±5% of the measured value; ±1.6 × 10^{-6} m^3·s^{-1}]

3. Characterization of the Experimental Facility Components

3.1. Airtightness of the Model

To ensure the model behaved like a real building during a pressurization measurement, this section presents the results of the characterization of the following parameters:

1. The airtightness of the model with sealed openings.
2. The airtightness of the model for all leakage distributions.
3. The airflow through each opening.

3.1.1. Airtightness of the Model with Sealed Openings

First, the airtightness of the model was evaluated without deliberate leaks. The model was subjected to a pressure difference of Δp = 200 Pa. Subsequent changes in pressure inside the model were analyzed once the pressurization stopped. Figure 6 provides a comparison of the decrease in the pressure inside the model, both with and without deliberate leaks. With only the smallest leak (1.7 mm diameter), the pressure inside the model dropped from 200 Pa to 0 Pa in less than 4 s. Without any deliberate leak, it took around 12 min to drop from 200 Pa to 10 Pa, showing the model's considerable airtightness.

3.1.2. Airtightness of the Model for the Nine Leakage Distributions

The airtightness of the model was then evaluated using the two openings across nine configurations of leakage distributions. Two methods were applied. For each configuration, the reference value at 4 Pa was evaluated twice: a first time according to the ISO 9972 method (from 10 to 100 Pa) and a second time by direct measurement of the airflow rate at 4 Pa (Table 5). For all the configurations, similar q_4 values were obtained for both methods,

with a maximum difference of 0.007 $m^3 \cdot h^{-1}$ (4%). Given the accuracy of the measurement device (5%), the differences might have arisen from the reliability of the measurement device or the reliability of the test method. For all the configurations, the average value for q_4 was 0.168 $m^3 \cdot h^{-1}$ with ISO 9972 and 0.167 $m^3 \cdot h^{-1}$ with the direct measurement at 4 Pa. These values corresponded to an effective leakage area (ELA_4) of 18.0 mm^2. This was significantly smaller than the value used to design the model, as described in Section 2.4 (22.7 mm^2). Such a discrepancy was influenced by the manufacturing accuracy and the assumptions regarding the Cd and Cp values. The model was more airtight. As the airtightness level did not significantly affect the impact of the wind during the measurements, this difference between the designed airtightness and the real airtightness of the model would not have an impact on future experiments, and the real value was used in the calculations.
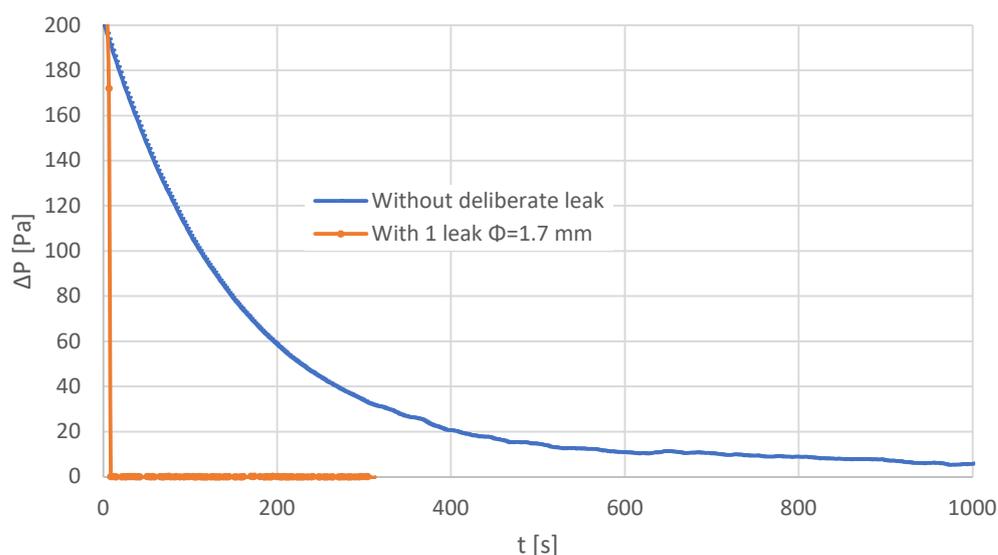

Figure 6. Characterization of the airtightness of the model without deliberate leaks and with the smallest leak observation of a pressure decrease inside the model.

Table 5. Evaluation of the real q_4 value of the model without wind with the same designed q_4 for all configurations.

r_{LD}	q_4 (ISO 9972) [$m^3 \cdot h^{-1}$]	q_4 (direct @4Pa) [$m^3 \cdot h^{-1}$]	Difference [$m^3 \cdot h^{-1}$]
0.1	0.175	0.170	0.005
0.2	0.167	0.167	0
0.3	0.163	0.163	0
0.4	0.166	0.167	−0.001
0.5	0.172	0.165	0.007
0.6	0.166	0.167	−0.001
0.7	0.163	0.163	0
0.8	0.167	0.167	0
0.9	0.175	0.170	0.005
Average	0.168	0.167	0.001

3.1.3. Airflow through Each Opening

To characterize the flow through each leak, fan pressurization tests were performed on the model with only one opening without wind. With the two smallest openings, the model was too airtight; it was impossible to induce pressure differences of less than 200 Pa, which was the saturation point of the manometer. For the remaining openings, a fan

pressurization measurement was performed according to ISO 9972 on the model with only one opening. The airflow coefficient C and the airflow exponent n were characterized for each of these openings. Table 6 gives the designed and the experimental values for the diameter, C, and n. The experimental value for the diameter was deduced from the experimental values of C and n, which were then used to calculate the leakage area and, subsequently, the opening diameter, according to Equation (19).

$$ELA_4 = \frac{1}{3600} * C * \frac{\rho_0^{0.5}}{2} * 4^{n-0.5} = A = \pi \frac{\varnothing^2}{4} \tag{19}$$

where ELA_4 is the evaluated effective leakage area at 4 Pa(m^2), C is the leakage coefficient (m$^3 \cdot$h^{-1} Pa^{-n}), n is the flow exponent (-), A is the area of the opening (m^2), and Φ is the diameter of the opening (m).

Table 6. Measured characteristics of the seven openings.

Designed Values			Experimental Values		
Diameter [10^{-3} m]	Flow Exponent n [-]	Flow Coefficient C [m$^3 \cdot$s^{-1} Pa^{-n}]	Diameter [10^{-3} m]	Flow Exponent n [-]	Flow Coefficient C [m$^3 \cdot$s^{-1} Pa^{-n}]
2.4	0.50	5.8×10^{-6}	2.5	0.54	5.6×10^{-6}
2.9	0.50	8.5×10^{-6}	3.0	0.53	8.3×10^{-6}
3.4	0.50	1.2×10^{-5}	3.4	0.53	1.1×10^{-5}
3.8	0.50	1.5×10^{-5}	3.8	0.52	1.4×10^{-5}
4.2	0.50	1.8×10^{-5}	4.1	0.51	1.7×10^{-5}
4.5	0.50	2.0×10^{-5}	4.4	0.50	1.9×10^{-5}
5.1	0.50	2.6×10^{-5}	5.0	0.49	2.5×10^{-5}

3.2. Pressure Coefficients on the Windward and Leeward Façades

The pressure coefficient at a specific point on the exterior façade depended on the wind speed, the reference pressure, and the pressure at that point, as shown in Equation (20).

$$C_p = \frac{2\left(p_{in} - p_{ref}\right)}{\rho_0 U^2} \tag{20}$$

where C_p is the wind pressure coefficient at the opening, ρ_0 is the outside air density (kg m^{-3}), U is the wind speed at the height of the building (m$\cdot$s^{-1}), p_{in} is the indoor pressure relative to the external pressure (Pa), and p_{ref} is the external reference pressure (Pa).

To evaluate the C_p value for each opening of the model, the pressure difference between inside the model and an external reference located in the testing chamber was measured for all wind speeds in the following configurations:

- A single 5.1 mm leak on the windward façade.
- A single 10 mm leak on the windward façade.
- A single 5.1 mm leak on the leeward façade.
- A single 10 mm leak on the leeward façade.

Figure 7 presents the C_p values evaluated according to Equation (20) for each configuration. The mean value for C_p at the windward (and correspondingly leeward) opening site was 0.42 (−0.57). The order of magnitude of these C_p values was consistent with the values given by Liddament [38]: +0.4 for the average value on the windward façade and −0.3 for the average value on the leeward façade.
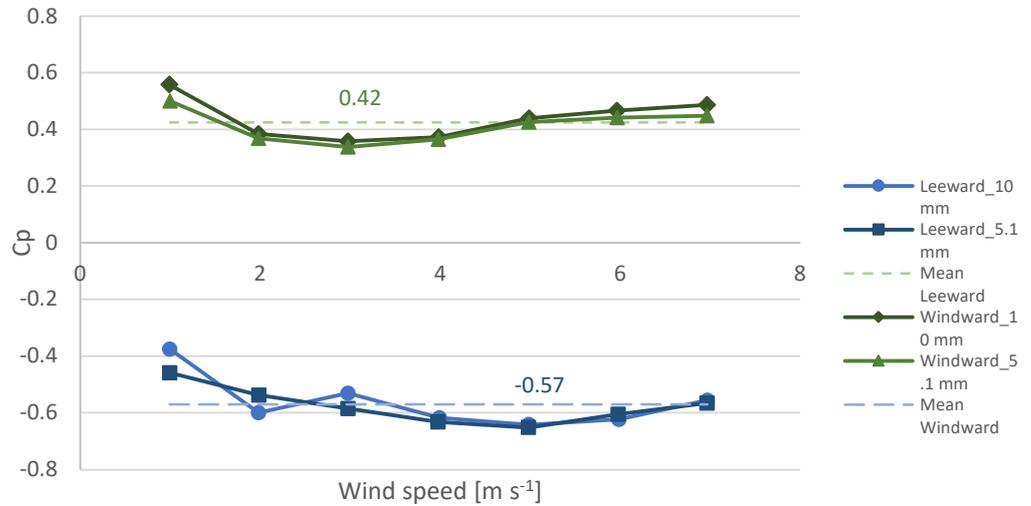
Figure 7. Evaluation of the Cp values on the opening site for a 10 mm and 5.1 mm leak.

3.3. Steady Wind Conditions in the Testing Chamber

The wind speed could be stabilized below 1 m·s^{-1} in the testing chamber and the maximum stabilized speed was 7.5 m·s^{-1}. To verify the homogeneity of the wind speed inside the testing chamber of the wind tunnel, velocity measurements were performed at 42 equally spaced locations covering the whole testing chamber (Figure 8). The wind velocity was measured at the height of the model, i.e., 0.25 m from the ground of the testing chamber, for different wind speed configurations for 1 min with one value per second. Figure 9 presents the results of the measurements performed for wind speeds between 4 and 5 m·s^{-1} from points A to E. The maximum standard deviation for the 42 locations during a one-minute measurement was 0.087 m·s^{-1} (anemometer accuracy: 0.2 m·s^{-1}), confirming the temporal stability of the wind speed for each location. Among the 42 averaged values of wind speeds, the minimum wind speed measured was 4.43 m·s^{-1}, and the maximal wind speed was 4.90 m·s^{-1}, indicating a maximal deviation of 10% for wind speeds in the testing chamber.
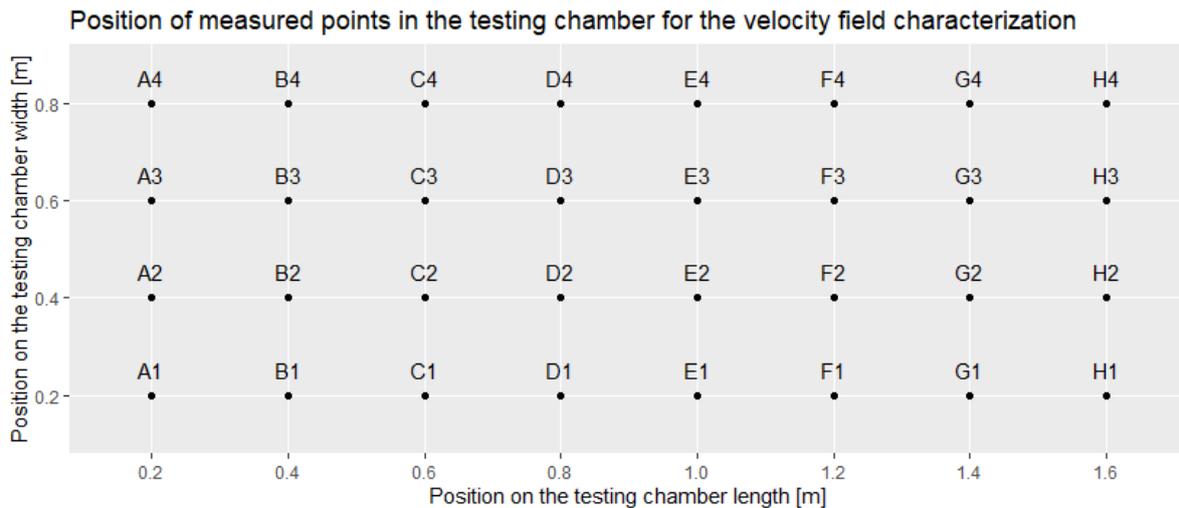

Figure 8. Schematic representation of the velocity field assessment points within the testing chamber (flow direction from A to H).
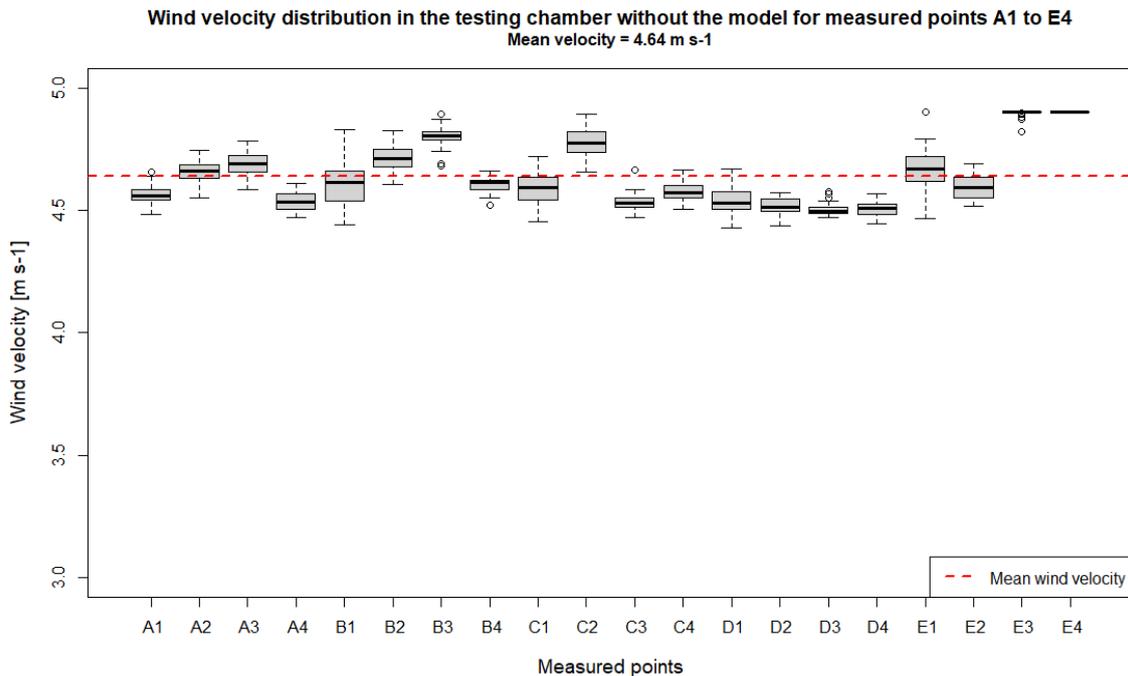
Figure 9. Distribution of the wind velocities in the testing chamber for a mean wind velocity = 4.64 m·s^{-1}—points A1 to E4.

4. Reproduction of ISO 9972 for Steady Winds in the Model Scale

The pressure taps for the internal pressure were located at the bottom of the model and inside the testing chamber. For this second tap, a T-pipe fitted at the end tubing was used. Regarding the zero-flow pressure measurement, a 60-s protocol of 30 measurements (one value every 2 s) was employed both before and after the pressure sequence.

For the pressure sequence, the following conditions needed to be met:

1. The lowest pressure difference respected the ISO 9972 requirement.
2. The highest pressure difference was 100 Pa.
3. The increment was 10 Pa.
4. The sequence included between 5 and 10 tests, depending on the lowest pressure difference.

Furthermore, each value of the pressure difference of the pressure sequence corresponded to an average of 10 values during 20 s (one value every 2 s). Recording started when three consecutive values met the pressure target (± 1 Pa) and the wind speed target (± 0.1 m·s^{-1}).

By combining the nine leakage distributions with the eight wind speeds (from 0 to 7 m·s^{-1}), 864 tests across 96 measurements were conducted. For each air leakage configuration and wind speed, fan pressurization measurements were performed according to ISO 9972 and with the parameters described in Section 3.1.1. When possible (depending on the zero-flow pressure), the pressure sequence included 10 tests. Appendix A represents the step-by-step experiment. Figure 10 provides plots of the maximum number of possible tests (grey bars) and the minimal values for the first step (blue line), depending on the wind speed (0 to 7 m·s^{-1}) and each air leakage distribution (r_{LD} from 0.1 to 0.9).

A large variability of the fan pressurization measurement results was observed depending on the air leakage distribution. The zero-flow pressure value could be very high when the leakage was mostly located on the leeward façade (rld < 0.5). For r_{LD} = 0.1 and r_{LD} = 0.2, the zero-flow pressures were higher than 16 Pa (5*zero-flow pressure higher than 80 Pa) at 7 m·s^{-1}, whereas the limit value in ISO 9972 was 5 Pa. Thus, only measurements for wind speeds up to 3 m·s^{-1} complied with the ISO 9972 requirements regarding zero-flow pressure. This was consistent with ISO 9972, which noted that a wind speed near the

ground above 3 m·s^{-1} will unlikely lead to a zero-flow pressure below 5 Pa. Conversely, the zero-flow pressure value was lower when the leakage was mostly located on the windward façade (rld > 0.5); from $r_{LD} = 0.7$ to $r_{LD} = 0.9$, the zero-flow pressure was higher than 5 Pa only when the wind speed was higher than 5 m·s^{-1}. However, a unique configuration for $r_{LD} = 0.6$ was observed; the zero-flow pressure was extremely low and stable, with a maximum value of 1 Pa at 7 m·s^{-1}. For this configuration, measurements according to ISO 9972 could be performed for all windy conditions. This seemed to correspond to a specific situation for which the pressure due to the wind is compensated for by the specific leakage distribution and the specific C_p coefficient of the model.
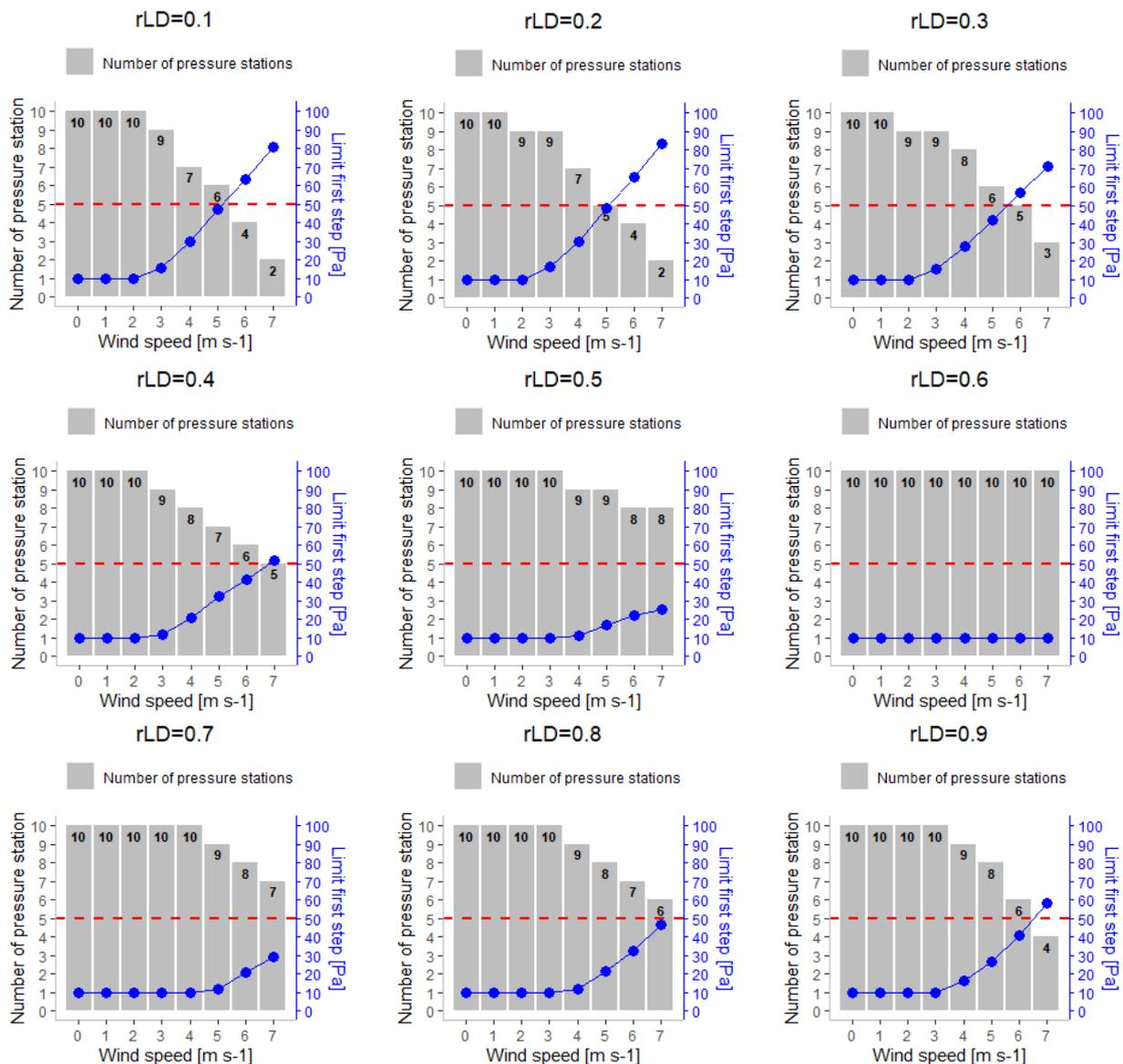
Figure 10. Number of pressure tests (stations) for a fan pressurization measurement depending on the wind speed for nine leakage distributions (red line = ISO 9972 constraint with at least 5 pressure stations).

Secondly, ISO 9972 required a minimum of five tests. Neglecting the 5 Pa limit for the zero-flow pressure and given that the first test had to be at least equal to five times the zero-flow pressure with an increment of 10 Pa, the maximum value for the first test was 60 Pa when the higher test was 100 Pa. This corresponded to a maximum zero-flow pressure of 12 Pa. When the leakage was mostly on the leeward side ($r_{LD} = 0.1$ to 0.3), it was not possible to perform fan pressurization measurements for high wind speeds, as the

zero-flow pressure was higher than 12 Pa and the pressure sequence could not include the minimum five tests. On the contrary, for $r_{LD} = 0.6$, all the measurements included 10 tests regardless of the wind speed.

To conclude, ISO 9972 pressurization measurements could be executed for many situations. However, when the leakage was mostly on the leeward side ($r_{LD} = 0.1$ to 0.3) with a high-velocity wind, the lowest pressure test could exceed 60 Pa, violating the minimum of five tests for the pressure sequence. This analysis also showed that the configuration ($r_{LD} = 0.6$) of the model corresponded to a very specific situation of balance; the impact of the wind for this situation would need to be carefully analyzed.

5. Discussions and Perspectives

The experimental facility presented in this study was designed to replicate fan pressurization measurements in line with ISO 9972. It was capable of performing measurements under pressure sequences up to 100 Pa for different steady wind conditions and nine leakage distributions, respecting the similarity conditions. This facility was developed to evaluate the uncertainty of the ISO 9972 protocol regarding wind impact. Specifically, the measurements were carried out under the following conditions:

- At a reduced scale.
- Under controlled laboratory conditions.
- In steady windy conditions up to $7 \, \text{m·s}^{-1}$.
- Without the stack effect.
- On a single-zone model with two circular leaks of different sizes.
- In the pressurization mode.

In order to isolate and quantify the errors attributable solely to the effects of steady wind in the experimental facility, future studies are needed. These should encompass a full characterization of the wind tunnel's dynamics, including both the wind speed and pressure fields, a comprehensive assessment of all the potential uncertainty sources, and an in-depth comparison with theoretical results [39].

While maintaining the similarity conditions, the model's leak characteristics (especially the size and shape) might have differed from real building leak behaviors. Moreover, the composition of the walls of the model did not reproduce the potential valve effects observed in full-scale buildings. The model also omitted the impact of internal partitions, which may induce disturbances on the air moving inside the building during a measurement, which was not taken into account in this study. Nine configurations of leakage distributions were considered, whereas an infinite number of distributions exist for real buildings. As this factor very significantly influences the error due to wind, the results of experimental evaluation using this model did not provide an exhaustive representation of what may occur on full-scale buildings.

Only steady wind conditions were reproduced, and wind fluctuations may induce larger errors than the mean speed value.

Since the measurements were performed with these conditions, the evaluation of the impact of the wind during the pressurization tests performed according to ISO 9972 with this experimental facility might not directly translate into practical corrections for real-world tests. Nevertheless, they can provide an order of magnitude of the error that can be induced by steady wind, and thus may highlight potential improvements in the measurement protocol.

Moreover, the facility's controlled environment allowed for repeatability measurements, enabling different analysis methods using the same experimental data. Therefore, the data and the experimental facility may be used in the future to better characterize the impact of the wind and improve its inclusion in the measurement protocol of ISO 9972. For large-scale building tests, precisely characterizing the wind during airtightness is time consuming and often impossible. However, understanding wind error through both experimental studies in laboratory conditions and theoretical analyses is crucial. This understanding can lead to either an adapted protocol to mitigate significant wind error (for

example, using different zero-flow pressure difference constraints, as suggested by Kölsch et al. [39], or applying a modified weighted regression, as proposed by Prignon et al. [21]) or to a consideration of different thresholds that account for probable uncertainty of the result. This uncertainty can be quantitatively evaluated in future studies.

As the model was scalable, future measurements can involve the following:

- Different types of leaks, incorporating different shapes, sizes, and n values.
- Integration insulation material.
- Adding more leaks. This will require performing a new similarity analysis and might lead to the modification of the experimental facility.

Another evolution of the experimentation would be to reproduce unsteady conditions, integrating factors like the stack effect by installing a heating system and insulation material in the model. Then, a comparison should be conducted between the experimental results at the model scale and the tests that are performed on different buildings under monitored wind conditions.

Beyond its current scope, the facility can be used for other studies. For instance, the wind tunnel is already being used to evaluate the impact of wind on water evaporation in new building components. Other applications regarding building measurements and ventilation device characterization might be used in the facility.

This study is linked to ongoing initiatives aimed at improving buildings' airtightness measurement reliability, particularly under the influence of external factors like wind and the stack effect. As highlighted by Kölsch et al. [27], there has been an effort to gather insights and address the limitations of current methodologies. This collaborative approach led to the formation of a working group focusing on identifying and resolving issues with the existing standards, such as ISO 9972. In 2023, the ISO committee responsible for ISO 9972 acknowledged the need for a revision of this standard, largely influenced by the collective input from this working group. The research presented in our paper is a significant contribution to this ongoing process. Specifically, our findings regarding the impact of wind velocity on airtightness measurements offer critical insights that can help refine the ISO 9972 standard. By providing empirical data and comprehensive analyses, our work supports the development of more accurate and stable methods for assessing building envelope airtightness. Moreover, the implications of our study extend to building energy performance [40]. Accurate airtightness measurements are fundamental for ensuring buildings meet energy efficiency criteria, as they directly impact heating and cooling loads. Improved measurement standards, influenced by our research, can lead to more reliable evaluations of building envelopes, facilitating better compliance with energy performance standards and contributing to overall energy conservation efforts in the building sector.

6. Conclusions

To evaluate the impact of wind on building airtightness measurements, an experimental facility was designed, reproducing fan pressurization measurements on a model-scale level. This facility included a model that represented a single-zone building with two adjustable leaks on two opposite façades, an air permeability measurement device capable of reproducing a fan pressurization measurement, and a wind tunnel that reproduced steady wind conditions. The design phase included a similarity analysis, ensuring the experimental results on the model scale would be consistent with real-scale physical phenomena.

The model was adjustable and provided nine configurations of leakage distribution between the windward and leeward façades, with the same averaged total airtightness for all configurations of $q_4 = 0.17$ m^3·h^{-1}. The airflow through each leak was characterized and corresponded to airflows through short leaks, comparable to an orifice (n = 0.5). With movable façades and openings, the model could adapt, incorporating more openings with different shapes and materials. The values of the pressure coefficient evaluated on the windward and leeward façade were in agreement with the documented values given in the literature.

The wind tunnel was 4.11 m long and included a $1.0 \times 1.0 \times 1.5$ m^2 testing chamber. The wind speed inside the testing chamber was homogeneous and could be stabilized from less than 1 m·s^{-1} to 7.5 m·s^{-1}. The wind velocity inside the testing chamber was very stable in time and in space.

In total, 96 fan pressurization measurements for the nine leakage distributions were performed on a model scale under wind speeds from 0 to 7 m·s^{-1}. All these measurements were performed using Labview applications and a VBA program was developed in this study to control the experimental facility and record all the output files. The zero-flow pressure difference, which is one of the major criteria to validate a test according to the ISO 9972 standard, was analyzed for all these tests. The results showed that variations in the zero-flow pressure difference induced by the wind strongly depended on the leakage distribution. Some notably low zero-flow pressure differences were obtained for strong winds, indicating the zero-flow pressure difference may not always be a reliable indicator of windy conditions.

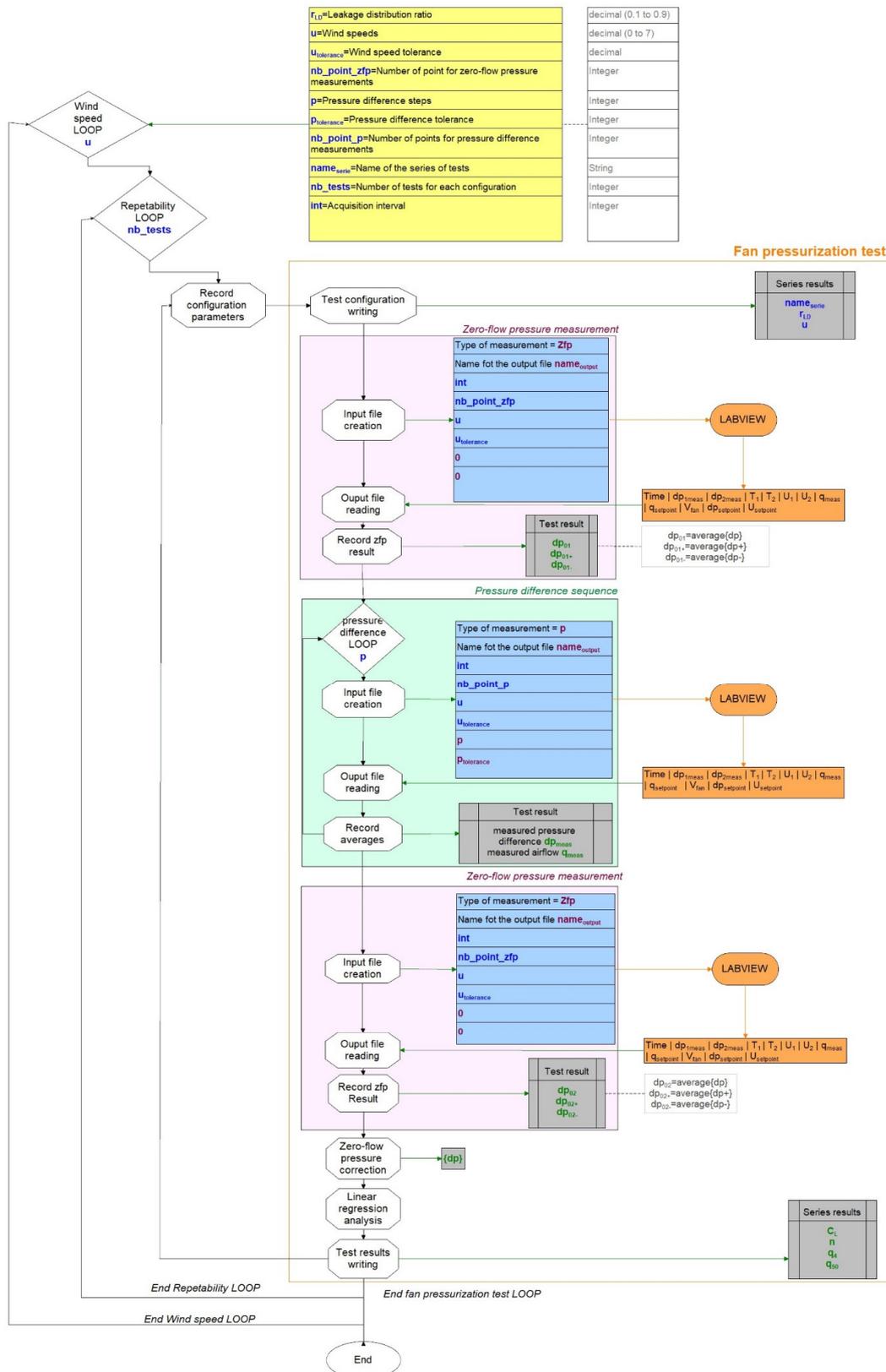# Appendix A. Representation of the Fan Pressurization Automation

Figure A1. Representation of the fan pressurization automation—Scheme of the VBA program that gives instructions to Labview apps.

References

1. European Parliament and Council. *Directive 2010/31/EU of 19 May 2010 on the Energy Performance of Buildings*; European Parliament and Council: Brussels, Belgium, 2010.
2. Amanowicz, Ł.; Ratajczak, K.; Dudkiewicz, E. Recent Advancements in Ventilation Systems Used to Decrease Energy Consumption in Buildings—Literature Review. *Energies* **2023**, *16*, 1853. [CrossRef]
3. Simson, R.; Rebane, T.; Kiil, M.; Thalfeldt, M.; Kurnitski, J. The Impact of Infiltration on Heating Systems Dimensioning in Estonian Climate. *E3S Web Conf.* **2020**, *172*, 05004. [CrossRef]
4. Poza-Casado, I.; Meiss, A.; Padilla-Marcos, M.Á.; Feijó-Muñoz, J. Airtightness and energy impact of air infiltration in residential buildings in Spain. *Int. J. Vent.* **2021**, *20*, 258–264. [CrossRef]
5. Poza-Casado, I.; Cardoso, V.E.M.; Almeida, R.M.S.F.; Meiss, A.; Ramos, N.M.M.; Padilla-Marcos, M.Á. Residential buildings airtightness frameworks: A review on the main databases and setups in Europe and North America. *Build. Environ.* **2020**, *183*, 107221. [CrossRef]
6. Moujalled, B.; Kölsch, B.; Mélois, A.; Leprince, V. Quantitative correlation between buildings air permeability indicators: Statistical analyses of over 400,000 measurements. *Energy Build.* **2023**, *298*, 113566. [CrossRef]
7. Kempton, L.; Daly, D.; Kokogiannakis, G.; Dewsbury, M. A rapid review of the impact of increasing airtightness on indoor air quality. *J. Build. Eng.* **2022**, *57*, 104798. [CrossRef]
8. *ISO EN ISO 9972*; Thermal Performance of Buildings-Determination of Air Permeability of Buildings-Fan Pressurization Method. International Organization for Standardization: Geneva, Switzerland, 2015.
9. *ASTM E779-19*; Standard Test Method for Determining Air Leakage Rate by Fan Pressurization. ASTM International: West Conshohocken, PA, USA, 2019. [CrossRef]
10. Walker, I.S.; Sherman, M.H.; Joh, J.; Chan, W.R. Applying Large Datasets to Developing a Better Understanding of Air Leakage Measurement in Homes. *Int. J. Vent.* **2013**, *11*, 323–338.
11. Love, J.; Wingfield, J.; Smith, A.Z.P.; Biddulph, P.; Oreszczyn, T.; Lowe, R.; Elwell, C.A. 'Hitting the target and missing the point': Analysis of air permeability data for new UK dwellings and what it reveals about the testing procedure. *Energy Build.* **2017**, *155*, 88–97. [CrossRef]
12. Nevander, L.E.; Kronvall, J. *Air Tightness of Buildings-Research in Sweden*; Air Infiltration and Ventilation Centre: Paris, France, 1978.
13. Mees, C.; Loncour, X. *Quality Framework for Reliable Fan Pressurisation Tests*; Qualicheck; Air Infiltration and Ventilation Centre: Paris, France, 2016.
14. Mélois, A.; Carrié, F.R.; El Mankibi, M.; Moujalled, B. Uncertainty in building fan pressurization tests: Review and gaps in research. *J. Build. Eng.* **2022**, *52*, 104455. [CrossRef]
15. Nolwenn Hurel, V.L. VIP 41: Impact of Wind on the Airtightness Test Results. Available online: https://www.aivc.org/resource/vip-41-impact-wind-airtightness-test-results (accessed on 4 January 2022).
16. Carrié, F.R.; Leprince, V. Uncertainties in building pressurisation tests due to steady wind. *Energy Build.* **2016**, *116*, 656–665. [CrossRef]
17. Delmotte, C. Airtightness of buildings–Assessment of leakage-infiltration ratio and systematic measurement error due to steady wind and stack effect. *Energy Build.* **2021**, *241*, 110969. [CrossRef]
18. Modera, M.P.; Wilson, D.J. The Effects of Wind on Residential Building Leakage Measurements. *Air Chang. Rate Airtightness Build.* **1990**, *1067*, 132. [CrossRef]
19. Delmotte, C.; Laverge, J. Interlaboratory tests for the determination of repeatability and reproducibility of buildings airtightness measurements. In Proceedings of the 32nd AIVC Conference, Brussels, Belgium, 12–13 October 2011.
20. Prignon, M.; Dawans, A.; Altomonte, S.; Van Moeseke, G. A method to quantify uncertainties in airtightness measurements: Zero-flow and envelope pressure. *Energy Build.* **2019**, *188–189*, 12–24. [CrossRef]
21. Prignon, M.; Delmotte, C.; Dawans, A.; Altomonte, S.; van Moeseke, G. On the impact of regression technique to airtightness measurements uncertainties. *Energy Build.* **2020**, *215*, 109919. [CrossRef]
22. Kölsch, B.; Walker, I.S. Improving air leakage prediction of buildings using the fan pressurization method with the Weighted Line of Organic Correlation. *Build. Environ.* **2020**, *181*, 107157. [CrossRef]
23. Kölsch, B.; Mélois, A.; Leprince, V. Improvement of the ISO 9972: Proposal for a more reliable standard to measure air leakage rate using fan pressurization method. In Proceedings of the 13th International BUILDAIR Symposium Airtight Buildings, Thermography and Ventilation Systems in Practice, Hanover, Germany, 2–3 June 2023.
24. Carrié, F.R.; Mélois, A.B. Modelling building airtightness pressurisation tests with periodic wind and sharp-edged openings. *Energy Build.* **2019**, *208*, 109642. [CrossRef]
25. Mélois, A.B.; Tran, A.D.; El Mankibi, M.; Carrié, F.R.; Moujalled, B.; Guyot, G. Designing a model-scale experiment to evaluate the impact of steady wind on building air leakage measurements. In Proceedings of the 40th AIVC Conference, Ghent, Belgium, 15–16 October 2019.
26. Mélois, A.B.; Tran, A.D.; Mankibi, M.E.; Carrié, F.R.; Moujalled, B.; Guyot, G. Assessment of wind impact on building air leakage measurements using a model scale experiment. In Proceedings of the E3S Web of Conferences, Tallinn, Estonia, 6–9 September 2020; EDP Sciences: Les Ulis, France, 2020; Volume 172, p. 05006. [CrossRef]
27. Le Roux, N. *Etude par Similitude de L'influence du Vent Sur les Transferts de Masse Dans les Bâtiments Complexes*; Université de La Rochelle, Laboratoire LEPTIAB: La Rochelle, France, 2011.

28. Ge, C. *Design, Construction and Characterization of a Wind Tunnel*; New Jersey Institute of Technology: Newark, NJ, USA, 2015.
29. Mauro, S.; Brusca, S.; Lanzafame, R.; Famoso, F.; Galvagno, A.; Messina, M. Small-Scale Open-Circuit Wind Tunnel: Design Criteria, Construction and Calibration. *Int. J. Appl. Eng. Res.* **2017**, *12*, 13649–13662.
30. Prandtl, L. Attaining a Steady Air Stream in Wind Tunnels. 1933. Available online: http://ntrs.nasa.gov/search.jsp?R=19930094 691 (accessed on 26 November 2019).
31. Gonzalez Hernandez, M.A.; Moreno Lopez, A.I.; Jarzabek, A.A.; Perales Perales, J.M.; Wu, Y.; Xiaoxiao, S. Design Methodology for a Quick and Low-Cost Wind Tunnel. In *Wind Tunnel Designs and Their Diverse Engineering Applications*; Ahmed, N., Ed.; InTech: Sydney, Australia, 2013; ISBN 978-953-51-1047-7.
32. Bell, J.H.; Mehta, R.D. Contraction Design for Small Low-Speed Wind Tunnels. 1988. Available online: https://ntrs.nasa.gov/search.jsp?R=19890004382 (accessed on 29 June 2019).
33. Choi, C.-K.; Kwon, D.K. Wind tunnel blockage effects on aerodynamic behavior of bluff body. *Wind. Struct. Int. J.* **1998**, *1*, 351–364. [CrossRef]
34. Uematsu, Y.; Isyumov, N. Wind pressures acting on low-rise buildings. *J. Wind Eng. Ind. Aerodyn.* **1999**, *82*, 1–25. [CrossRef]
35. Walker, I.S.; Wilson, D.J.; Forest, T.W. Wind Shadow Model for Air Infiltration Sheltering by Upwind Obstacles. *HVACR Res.* **1996**, *2*, 265–282. [CrossRef]
36. Guyot, G.; Ferlay, J.; Gonze, E.; Woloszyn, M.; Planet, P.; Bello, T. Multizone air leakage measurements and interactions with ventilation flows in low-energy homes. *Build. Environ.* **2016**, *107*, 52–63. [CrossRef]
37. *ASHRAE 2009*; ASHRAE Handbook–Fundamentals: SI Editions. American Society of Heating, Refrigerating and Air-conditioning Engineers, Inc.: Atlanta, GA, USA, 2009.
38. Liddament, M.W. *A Guide to Energy Efficient Ventilation-AIC-TN-VENTGUIDE-1996*; Air Infiltration and Ventilation Centre: Ghent, Belgium, 1996; 254p.
39. Kölsch, B.; Leprince, V.; Mélois, A.; Moujalled, B. Reassessing ISO 9972 constraints: A mathematical analysis of errors in building airtightness tests due to steady wind and stack effect. *Energy Build.* **2024**, *305*, 113873. [CrossRef]
40. Hurel, N.; Leprince, V. VIP 46: Building Airtightness Impact on Energy Performance (EP) Calculations. 2023. Available online: https://www.aivc.org/resource/vip-46-building-airtightness-impact-energy-performance-ep-calculations (accessed on 15 January 2024).